DETAILED CHARACTERIZATION OF A FIVE-DIMENSIONAL PHASE SPACE DISTRIBUTION*

A. Hoover†, K. Ruisard, A. Aleksandrov, A. Zhukov, S. Cousineau
Oak Ridge National Laboratory, Oak Ridge, TN, USA

Abstract

There are two primary uses of phase space distribution measurements in particle accelerators. (i) *Analysis*: features in the phase space distribution are identified and explained. (ii) *Prediction*: particles are sampled from the distribution and propagated through an accelerator model. Both tasks are non-trivial in high-dimensional phase space. Here, we outline our approach to these problems for a high-resolution five-dimensional phase space measurement at the Spallation Neutron Source (SNS) Beam Test Facility (BTF).

INTRODUCTION

Research at the Spallation Neutron Source (SNS) Beam Test Facility (BTF) is aimed at predicting the evolution of intense hadron beams at the halo level [1]. As part of this effort, high-dimensional and high-dynamic-range phase space measurements have been pioneered at the BTF. The first six-dimensional (6D) measurement was performed at low resolution as a proof of principle [2]; subsequent studies have explored various projections and slices of the 6D distribution in higher resolution and dynamic range [3–6].

Note that the predictive task stated above does not require analysis of the measured distribution; it only requires that the distribution be input to a computer simulation. Thus, we may identify two related but separate uses of phase space measurements: (i) *Analysis*: features in the distribution are identified and explained. (ii) *Prediction*: particles are sampled from the distribution and propagated through an accelerator model. While previous research at the BTF has focused primarily on (i), ongoing research is focused on (ii).

Both tasks (i) and (ii) are non-trivial when the phase space is high-dimensional. In this paper, we outline the approaches we have used (or plan to use) to address these issues for high-dimensional measurements at the BTF. We focus on a recent high-resolution 5D measurement in which the distribution of longitudinal positions was ignored to enable a dense measurement grid ($\approx 64^5$) and high dynamic range ($\approx 10^3$) relative to full 6D measurements. A detailed analysis of this measurement is contained in [6], and the data is publicly available at https://doi.org/10.5281/zenodo.7517346. This paper can be considered supplementary material for [6].

VISUALIZATION

A measured phase space distribution encodes information about the beam dynamics preceding the measurement. Decoding this information is challenging since 2D projections mask relationships between three or more variables. This is illustrated in Fig. 1, which represents a 4D slice of $f(x, x', y, y', w)$, our measured 5D distribution. Here x and y are the transverse positions, x' and y' are the transverse slopes, and w is the deviation from the synchronous particle energy. The projection onto the x-x' plane is shown on the bottom right. This projection can be unraveled along the y/y' axis, generating the 3D distribution in the bottom row/right column. Each 3D projection can be unraveled along the remaining axis, generating the 4D distribution in the main panel.

The "slice matrix" plot in Fig. 1 uses planar slices of the distribution to visualize the dependence between the transverse phase space variables. One important feature is the bimodal x distribution near $y = 0$ in the bottom row. This feature appears near the synchronous particle energy ($w = 0$). In 5D, we observe this hollowing in $f(x, y, w)$, which we expect, due to the strongly correlated longitudinal phase space at the measurement plane ($z \approx w$), corresponds to a spatial hollowing of the 3D distribution $f(x, y, z)$. In [6], we argue that nonlinear space charge forces between the RFQ and the measurement plane drive this hollowing.

Hollowing is also visible in different subspaces. Cathey et al. [2] discovered a bimodal energy distribution near the center of the transverse phase space — a nonlinear correlation between all five phase space variables. Ruisard et al. [3, 4] studied this feature in greater detail, benchmarking against particle-in-cell simulations. We are reasonably certain that the feature develops in the RFQ, although we do not yet fully understand the underlying dynamics.

Slice matrices like Fig. 1 can be used to explore the transverse-energy relationship; however, these figures require a plethora of subplots and are constrained to 4D slices of the 5D distribution. Motivated by this difficulty, we have developed a method of non-planar slicing. The method is a generalization of a radial density plot, where the density on a sphere of radius r is plotted as a function of r. Here, $r^2 = \mathbf{x}^T\mathbf{x}$ for coordinate vector $\mathbf{x} = [x_1, \ldots, x_D]^T$; ellipsoids may be used instead of spheres to account for linear correlations in the data, in which case $r^2 = \mathbf{x}^T\boldsymbol{\Sigma}^{-1}\mathbf{x}$ for covariance matrix $\boldsymbol{\Sigma}$. Our proposal is to display the distribution in one subspace on a surface in a different subspace.

* This manuscript has been authored by UT- Battelle, LLC under Contract No. DE-AC05-00OR22725 with the U.S. DOE. The US government retains and the publisher, by accepting the article for publication, acknowledges that the US government retains a nonexclusive, paid-up, irrevocable, worldwide license to publish or reproduce the published form of this manuscript, or allow others to do so, for US government purposes. DOE will provide public access to these results of federally sponsored research in accordance with the DOE Public Access Plan (http://energy.gov/downloads/doe-public-access-plan).

† hooveram@ornl.gov

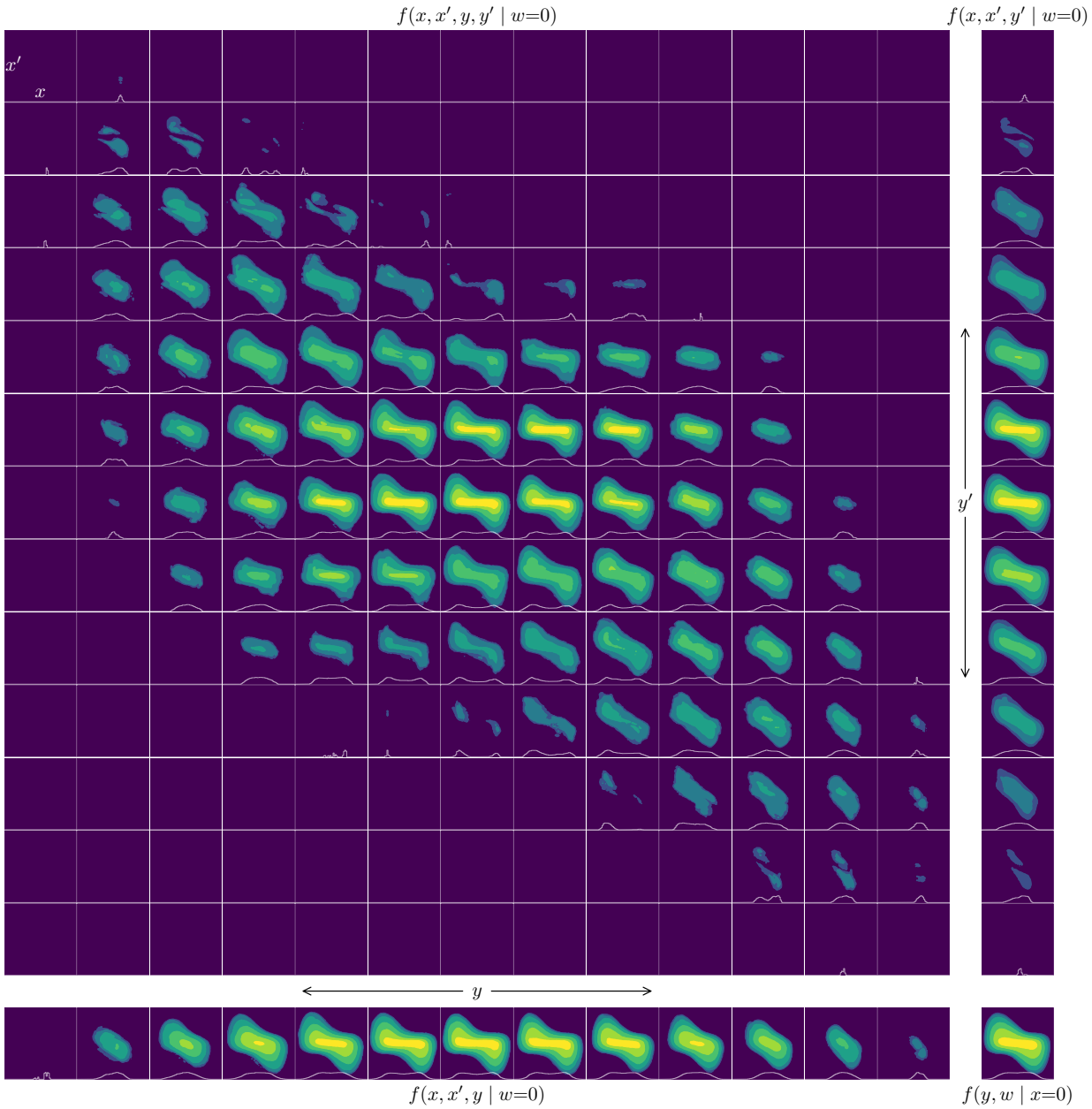

Figure 1: Dependence of the x-x' distribution (near $w = 0$) on y and y'. The subplots corresponding to each distribution share the same color map. The following density contours are displayed: $10^{-3.0}$, $10^{-2.5}$, $10^{-2.0}$, $10^{-1.5}$, $10^{-1.0}$, $10^{-0.5}$.

For example, one could define surfaces of radius r in the x_3-...-x_D plane, then visualize the x_1-x_2 distribution, integrated over each surface, as a function of r; i.e., compute $f(r(x_3, \ldots, x_D), x_1, x_2)$. If $f(x_3, \ldots, x_D)$ has ellipsoidal symmetry, the low-dimensional distribution will be sufficient to characterize the dependence of the x_1-x_2 distribution on the amplitude in the x_3-...-x_D plane. We call these slices *non-planar* to distinguish them from conventional slices, which are defined by the intersection of orthogonal (D-1)-dimensional planes.

Other surfaces, such as surfaces of constant density, can be used if the projections lack ellipsoidal symmetry; in the example above, the ellipsoids in the x_3-...-x_D plane would be replaced by the density contours of $f(x_3, \ldots, x_D)$. The surfaces can also be generalized to volumes, e.g., by selecting the region between two nested ellipsoids. In Fig. 2, we apply non-planar slices to our 5D distribution, mapping the dependence of the y-w distribution on x-x'-y'. Each subplot is the projection within a "shell slice" defined by two density contours of $f(x, x', y')$. The slice selects large-amplitude particles on the left and small-amplitude particles on the right. The energy distribution transitions smoothly from unimodal to bimodal.

Non-planar slices may also be used to interpret simulation data. Since 6D histograms are typically very sparse, many particles are needed to view multi-dimensional features such

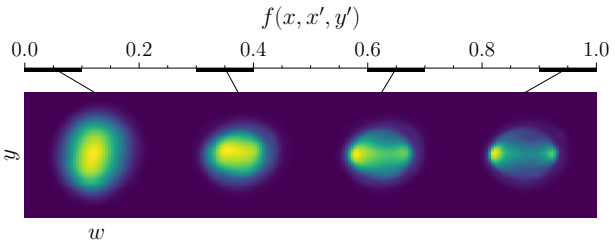

Figure 2: The y-w distribution as a function of the density in the x-x'-y' plane. The top row displays the density range corresponding to each y-w projection, with $f(x, x', y)$ normalized to the range [0, 1].

as the hollowing described above. Non-planar slices may increase the visibility of such features with fewer particles. They may also simplify the visualization of the beam halo in four- or six-dimensional phase space.

RECONSTRUCTION

To use phase space measurements for predictive purposes, we must be able to draw samples from a distribution function that is consistent with our data. In this section, we briefly chart our progress on this topic.

Interpolation

For simplicity, we neglect the finite slit widths and assume the measurement data is a set of intensities $\{f(\mathbf{x}_1), \ldots, f(\mathbf{x}_N)\}$, where $\mathbf{x} = [x, p_x, \ldots]^T$ is the D-dimensional phase space coordinate vector. The reconstruction of the phase space distribution $f(\mathbf{x})$ is an interpolation problem. Linear interpolation is (in our experience) infeasible for large data sets when $D > 3$. Fortunately, the points $\{\mathbf{x}_i\}$ are often on (or almost on) a regular grid, allowing us to build enormous density arrays from a series of 1D interpolations.

Unstructured data could result from irregular (non-rectilinear) scan patterns. Irregular scan patterns have been suggested (although not yet pursued) to reduce the execution time of 6D scans. Thus, it may be desirable to develop a more general interpolation method. We are considering two approaches. The first approach is to train a neural network to predict the density $f(\mathbf{x})$ at point $\mathbf{x}$. This straightforward approach shows promise in 3D; further testing is required for larger data sets. Another approach is to fit a normalizing flow [7] to the data. This approach is attractive because sampling from a normalizing flow is trivial. Normalizing flows are usually trained on sample data or a known distribution function rather than a discrete number of intensity measurements. Initial attempts to train a continuous normalizing flow on such data have been unsuccessful, but further investigation is warranted.

Combining measurements

If the 6D distribution is not measured directly, it must be reconstructed from lower dimensional projections. The simplest case is when the projections are independent, i.e., $\{f(x, p_x), f(y, p_y), f(z, p_z)\}$. More interesting cases occur when the projections share coordinates or represent non-orthogonal planes. As a practical example, consider the problem of combining $f(x, p_x, y, p_y, p_z)$ with $f(z, p_z)$ — both of which can be measured at much higher resolution than the full 6D distribution at this time.

The example just mentioned has the following maximum-entropy solution:

$$f(x, p_x, y, p_y, z, p_z) = f(x, p_x, y, p_y, p_z) \frac{f(z, p_z)}{f(z)}. \quad (1)$$

A memory-efficient way to obtain this solution is to sample points $\{x_i, p_{x_i}, y_i, p_{y_i}, p_{z_i}\}$ from $f(x, p_x, y, p_y, p_z)$, interpolate $f(z, p_z)$ to obtain $f(z \mid p_{z_i})$, then sample z_i from $f(z \mid p_{z_i})$. This method preserves the detail in the 5D measurement and extends to other projections involving z, such as $f(x, p_x, z, p_z)$. Although Eq. (1) does not inject correlations between z and the transverse phase space coordinates, it may suffice for BTF studies due to the absence of longitudinal focusing in the BTF lattice.

A general solution to the "in-place" reconstruction problem may be possible using variants of recently proposed tomography algorithms. In [8], a neural network was trained to predict the 4D distribution from compressed 2D projections; perhaps such a model could be extended to 6D. Alternatively, training a generative model on projections may be possible, as in [9]. There are various issues facing this type of reconstruction that we do not mention here.

Sampling

Once a distribution function $f(\mathbf{x})$ is known, we must draw samples from it. The simplest solution is *grid sampling*, where $f(\mathbf{x})$ is evaluated on a regular grid and treated as a histogram. Bins are randomly selected under the discretized distribution function and samples are drawn from a uniform distribution within each bin. This eventually produces a "checkerboard" density. The checkerboard effect can be reduced by using a high grid resolution and adding noise to the samples. This method has been tested on our high-resolution 5D measurement. Grid sampling is not ideal for typical measurements when $D = 6$ due to severe limitations on the grid resolution. Normalizing flows, which have been used to represent complex, high-dimensional Boltzmann distributions [10], are a promising alternative.

REFERENCES

[1] Z. Zhang, S. Cousineau, A. Aleksandrov, A. Menshov, and A. Zhukov, "Design and commissioning of the beam test facility at the spallation neutron source," *Nuclear Instruments and Methods in Physics Research, Section A: Accelerators, Spectrometers, Detectors and Associated Equipment*, vol. 949, Jan. 2020, ISSN: 01689002. DOI: 10.1016/j.nima.2019.162826.

[2] B. Cathey, S. Cousineau, A. Aleksandrov, and A. Zhukov, "First six dimensional phase space measurement of an accelerator beam," *Physical Review Letters*, vol. 121, 6 Aug. 2018, ISSN: 10797114. DOI: 10.1103/PhysRevLett.121.064804.

[3] K. Ruisard, A. Aleksandrov, S. Cousineau, V. Tzoganis, and A. Zhukov, "High dimensional characterization of the longitudinal phase space formed in a radio frequency quadrupole," *Physical Review Accelerators and Beams*, vol. 23, 12 Dec. 2020, ISSN: 24699888. DOI: 10.1103/PhysRevAccelBeams.23.124201.

[4] K. Ruisard and A. Aleksandrov, "Rapid charge redistribution leading to core hollowing in a high-intensity ion beam," *Physical Review Accelerators and Beams*, vol. 24, 1 Jan. 2021, ISSN: 24699888. DOI: 10.1103/PhysRevAccelBeams.24.014201.

[5] A. Aleksandrov, S. Cousineau, K. Ruisard, and A. Zhukov, "First measurement of a 2.5 mev rfq output emittance with 1 part-per-million dynamic range," *Nuclear Instruments and Methods in Physics Research, Section A: Accelerators, Spectrometers, Detectors and Associated Equipment*, vol. 987, Jan. 2021, ISSN: 01689002. DOI: 10.1016/j.nima.2020.164829.

[6] A. Hoover, K. Ruisard, A. Aleksandrov, S. Cousineau, and A. Zhukov, *Analysis of a hadron beam in five-dimensional phase space*, 2023. arXiv: 2301.04178 [physics.acc-ph].

[7] G. Papamakarios, E. Nalisnick, D. J. Rezende, S. Mohamed, and B. Lakshminarayanan, "Normalizing flows for probabilistic modeling and inference," *The Journal of Machine Learning Research*, vol. 22, no. 1, pp. 2617–2680, 2021.

[8] A. Wolski, M. A. Johnson, M. King, B. L. Militsyn, and P. H. Williams, "Transverse phase space tomography in an accelerator test facility using image compression and machine learning," *Phys. Rev. Accel. Beams*, vol. 25, p. 122 803, 12 Dec. 2022. DOI: 10.1103/PhysRevAccelBeams.25.122803. https://link.aps.org/doi/10.1103/PhysRevAccelBeams.25.122803

[9] R. Roussel *et al.*, "Phase space reconstruction from accelerator beam measurements using neural networks and differentiable simulations," *Phys. Rev. Lett.*, vol. 130, p. 145 001, 14 Apr. 2023. DOI: 10.1103/PhysRevLett.130.145001. https://link.aps.org/doi/10.1103/PhysRevLett.130.145001

[10] V. Stimper, B. Schölkopf, and J. M. Hernández-Lobato, "Resampling base distributions of normalizing flows," in *International Conference on Artificial Intelligence and Statistics*, PMLR, 2022, pp. 4915–4936.